ANALYSIS OF TARSAL TUNNEL SYNDROME USING IMAGE CORRELATION

Amarjot Singh[1] and S.N. Omkar[2]

[1]Department of Electrical and Electronics Engineering, National Institute of Technology, Warangal, India
E-mail: amarjotsingh@ieee.org
[2]Department of Aerospace Engineering, Indian Institute of Science, Bangalore, India
E-mail: omkar@aero.iisc.ernet.in

Abstract

Tarsal tunnel syndrome (TTS), also known as posterior tibial neuralgia is a painful disorder of the foot. It is a medical condition arising due to the compression of the tibial nerve in the tarsal tunnel, resulting in numbness, parenthesis and muscle weakness in foot. A number of imaging methodologies such as ultrasound as well as MRI imaging has been used in the past in order to analyze the strain pattern of gastrocnemius tendon and aponeurosis from the surface of the skin without analyzing the internal tendons. The DIC code developed, computes the in-plane strain with a correlation function using pictures taken before and after stretching, using a CCD camera. The shift between the initial picture and subsequent one is evaluated by cross-correlation using FFT. This paper gives in detail description of the preprocessing steps necessary to extract Zone of Interest from the two images. The effects of stretching on the superficial components of the tibial nerve, the posterior tibial artery and vein, and the tibialis posterior, flexor digitorum longus and flexor hallucis longus tendons in the calf and foot are studied.

Keywords:

Tarsal Tunnel Syndrome, Image Correlation, Fast Fourier Transform, Strain Analysis, Cross Correlation, Tibialis Posterior, Flexor Digitorum Longus, Flexor Hallucis Longus Tendons

1. INTRODUCTION

Tarsal tunnel syndrome (TTS), also called as posterior tibial neuralgia, is a painful disorder of the tarsal tunnel and foot [1]. TTS is a compression neuropathy and a painful foot condition in which the tibial nerve is compressed as it travels through the tarsal tunnel. The tarsal tunnel is made up of bone on the inside and the flexor retinaculum on the outside. This tunnel is located along the inner calf behind the medial malleolus (bump on the inside of the tarsal tunnel). Nerves in a bundle namely the posterior tibial artery, tibial nerve, and tendons of the tibialis posterior, flexor digitorum longus, and flexor hallucis longus muscles travel this pathway, through the tarsal tunnel. TTS can lead to numbness in the foot, pain, burning, electrical sensations, big toe and tingling over the base of foot and heel. The flexor retinaculum has a limited ability to stretch, so increased pressure will eventually cause compression on the nerve within the tunnel. With the increase in pressure on the nerves, the blood pressure decreases leading to tingling and numbness. The effect of the entrapment can spread to other area depending upon the locked area. If the entrapment is high, the entire foot can be affected as varying branches of the tibial nerve can become involved. TTS is mainly observed in athletes or sports persons due to the pressure applied by them on the tarsal tunnel such as tennis calf [2]. Such conditions can cause damage to the tendons passing through the foot leading to swelling and severe pain.

A number of techniques are being used for the treatment of TTS. The major remedies or physical exercises include Nerve tension test [3], calf stretching exercise [4] and sometimes surgical [5] release of the transverse tarsal ligament are often used to cure the syndrome. Since the effects of all the factors can be studied by the variations in foot postures, the author aims to come up with a method to analyze the stretch in tendons of the foot without any dependence of specialist. The author aims at using digital imaging to analyze and assist diagnosis for compression in the tarsal tunnel by computing the strain field on the superficial muscles and tendons of the top surface of leg.

Digital Imagery has being used over a number of years to compute and evaluate strain for a number of applications. 1-d time delay estimation techniques were used initially for displacement and strain estimation [6] while the evaluation of 2-d strain has been developed, using both B-mode data [7] and raw radio frequency (rF) data [8]. These strain-imaging techniques are being used primarily for cardiovascular applications [9] and breast and prostate tumor research [10]. A number of groups have been exploring the opportunity of shear strain imaging and its possible applications [11]. For instance, shear strain imaging has been of interest for characterization of breast tumors [12] and cardiovascular applications [13]. Rotation and, especially, torsion are of great interest in cardiovascular research [14]. Apart from the biomedical application, digital imaging has made its mark in a number of other applications including the measurement of deformation and strain in sheet metal forming analysis, automotive crash testing, rail vehicle safety [15], air-plane safety [16] etc. The methodology is also applied for quantitative evaluation of in-plane deformation characteristics of geo-materials [17], and also in medical fields to evaluate local failure of bone [18].

In the past, the measurement of strain was restricted to a specified location or discrete target points in a structure i.e. it was impossible to compute the strain distribution over the whole structure. A number of false attempts were made to extract data at a very large number of locations by using discrete targets due to the time consuming process and computational power requirements. A few techniques such as Moiré Interferometry [19], holographic Interferometry [20], speckle photography [21] have been proposed to acquire the overall deformation contour, but it is often time consuming and involves heavy computational power. On the other hand, Digital Image Correlation (DIC) is a simple and quick state-of-art technique superior to previous techniques due to its ability to compute faster.
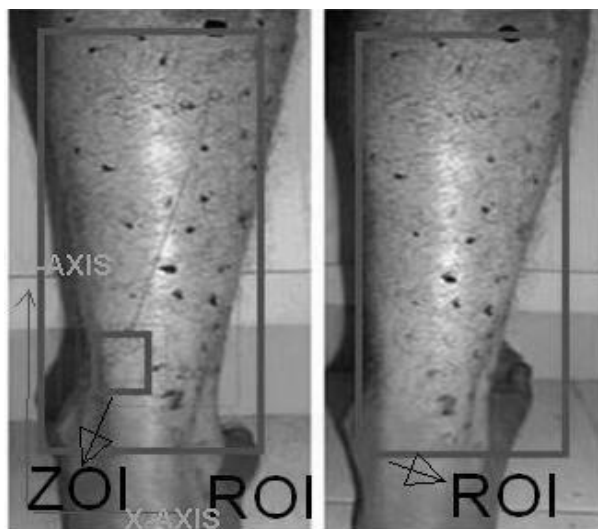
Fig.1. Calf Stretching Experiment: (a) Reference Image; (b) Deformed Image

DIC was originally introduced in the early '80s by researchers from the University of South Carolina [23]. The idea behind the method was to infer the displacement of the material under test by "tracking the deformation of a random speckle pattern applied to the component's surface in digital images acquired during the experiment" [22]. In addition to its non–contact, non destructive and full field measurement capability, the 2-D DIC technique is also well known for its simplicity, low environmental vulnerability and easy processing. A large number of algorithms [25] have been developed over the years in order to find the solutions through DIC. Among these methods, the most commonly used algorithm involves an iterative solution that finds the maximum of the cross-correlation coefficient in parameter space [33]. A correlation function is used to calculate the shift between the two images. The algorithm is highly effective when precise displacement between two images have to be calculated. Digital Image correlation has proven to be an extremely effective optical approach with vast applications like determining mechanical properties of human soft tissue in vivo [26], direct measurement of two-dimensional strain distributions within articular cartilage under unconfined compression [27], measuring Osteocyte lacunae tissue strain in cortical bone [28], determining local mechanical conditions within early bone callus [29] etc. DIC has been used to analyze the stresses in solder interconnects of BGA packages under thermal loading [30], [31] material characterization under thermal loading [32], dynamic testing to study deformation for flexible bodies [34], material characterization at high strain rate [35], stresses and strain in flip-chip die under thermal loading [36] etc.

DIC has been applied multiple times in the past in the field of applied anthropology to assist practitioners for diagnosis [41]. DIC has been effectively used to study the mechanical properties of biological soft tissues e.g. using 2D DIC: on the human tympanic membrane [37], sheep bone callus [29], human cervical tissue [38] and recently also using 3D DIC: for the bovine cornea [39] and mouse arterial tissue [40]. A number of algorithms have been developed and applied to evaluate the strain pattern due to the force applied on different body parts. A correlation function can be used to calculate the shift between

the two images taken before and after the deformation by tracking the speckle pattern, leading to evaluation of strain. The computation of cross-correlation can be performed in the physical space [42] or in the Fourier space using Fast Fourier Transform (FFT) [43]. The intermediate cross correlation FFT step can involve heavy computations depending upon the field due to the heavy computational complexity of the speckle pattern [44], [45], [46]. Digital Image Speckle Correlation (DISC) uses digital image correlation to resolve displacement and deformation gradient fields [47], [48], [49]. The underlying principle of DISC consists of tracking a geometric point before and after deformation resulting in its displacement vector.

The aim of the paper is to analyze the calf stretching, a remedy for TTS, through a non contact optical technique of Digital Image Correlation (DIC). The focus of the experiment is to examine the strain pattern on the superficial muscles of the leg as result of calf stretching. Calf stretching results in relaxation of the leg muscles. When the calf is stretched, the tarsal tunnel expands resulting into the expansion of the tendons which further leads to the relaxation. The effects of stretching on the superficial components of the calf muscles, namely the tibial nerve, the posterior tibial artery and vein, tibial nerve, the posterior tibial artery and vein, and the tibialis posterior, flexor digitorum longus, and flexor hallucis longus tendons in the calf and foot are studied. This can be of significance in further clinical studies.

2. PROBLEM FORMULATION AND EXPERIMENTATION

This setup consists of a desktop computer, a digital camera and the code used to compute the variations with calf stretching. The two dimensional variations are measured using the digital image correlation code written by the authors. The position of the camera and the subject are fixed for both pre and post images. The test was conducted on five healthy and active males with no known records of neural/muscular/skeletal disorders. Informed consent was obtained from each participant before the experiment was conducted. The average age, body height and body mass of the participants are 35.5 years, 170 cm and 68.5 kg respectively.

The experiment is started by coating the body part (right forearm anterior / right leg posterior) with zinc powder in order to provide contrast for better identification of marker points. Later, the zinc coated portion is covered with a random black speckle pattern with a marker. The subject is made to sit on a chair and place the leg at the so that view for the camera is not obstructed. Initially the calf muscle is in the relaxed position in Fig.1(a). A CCD camera is used to take the picture, referred to as reference image, of the calf muscle. In the next step, the calf muscle is stretched by lifting the foot approximately at angle of 45 degree above the ground; the deformed image as shown in Fig.1(b). The same setup is used to capture the picture, referred to as deformed image, in the extended position. Finally, the images captured are used for strain computation. The effects of stretching on the superficial components of the arm muscles, namely the flexor tendons in the calf, are studied.
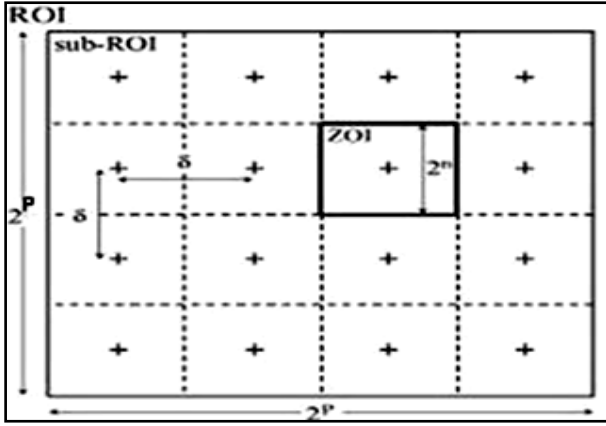
Fig.2. Schematic of the reference image with the parameters (Q = P and shift δ)
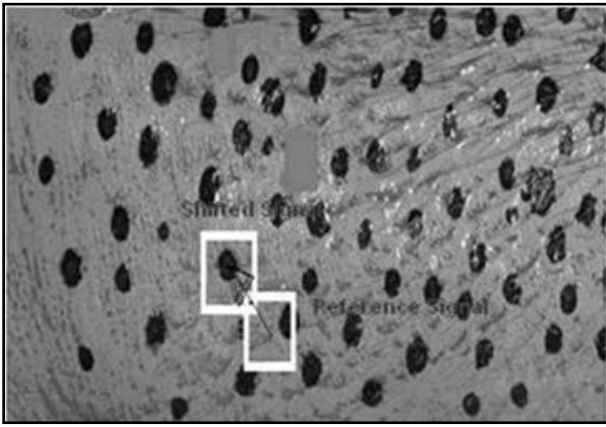

Fig.3. Movement of Zone of Interest from reference position to deformed position

Feature point extraction is the primary step in order to compute the strain pattern. Basic image processing operation of dilation is used in order to extract the feature points from the image. Further, the aim of the algorithm is to match the Zone of Interest of the reference image with the deformed image using a cross correlation function to evaluate the strain. FFT convolution is used in order to compute the strain for the feature points. The experiment is then repeated for five other subjects and the trends are observed.

3. DISPLACEMENT FIELD MEASUREMENT BY DIGITAL IMAGE CORRELATION

DIC is based on image matching algorithm. It can be effectively used in Fourier as well as physical space. The displacement field can be calculated by taking the correlation of an interrogation window of the deformed image with respect to the reference image.

3.1 PRELIMINARIES: CORRELATION OF TWO IMAGES

To determine the displacement field of one image of the deformed surface with respect to reference image, one considers a sub-image which will be referred to as a Zone of Interest (ZOI)

Fig.2. The purpose of the correlation method is to match the ZOIs in the respective images. The displacement of a ZOI with respect to its copy in deformed image is a two-dimensional shift of an intensity signal digitized by a camera. The aim is to locate the strain signal $g(\xi, \psi)$, (ZOI in the deformed image) a shifted copy of reference signal $f(\xi, \psi)$ (ZOI in the reference image) in order to compute the strain as shown in Fig.3. $g(\xi, \psi)$ can also be considered as equivalent to the reference signal $f(\xi, \psi)$ shifted by δ_x, δ_y. The strain function can be defined as,

$$g(\xi, \psi) = f(\xi - \delta_x, \psi - \delta_y) + b(\xi, \psi) \tag{1}$$

where, δ_x, δ_y are unknown displacement vectors and $b(\xi, \psi)$ a random noise. To evaluate the shift (δ_x, δ_y) one may minimize the norm of the difference between $f(\xi - x, \psi - y)$ and $g(\xi, \psi)$ with respect to x and y,

$$\min_{x,y} \| g(\bullet) - f(\bullet - x, \bullet - y) \|^2 \tag{2}$$

where, '•' is a dummy parameter. If one chooses the usual quadratic norm $\|f\|^2 = \int\limits_{-\infty}^{+\infty}\int\limits_{-\infty}^{+\infty} f(\xi, \psi) \partial \xi d\psi$, the previous minimization problem is equivalent to maximizing the quantity

$$h(x, y) = (g * f)(x, y)$$
$$= \int\limits_{-\infty}^{+\infty}\int\limits_{-\infty}^{+\infty} g(\xi, \psi) f(\xi - x, \psi - y) \partial \xi \partial \psi \tag{3}$$

where, '$*$' denotes the cross-correlation operator. Furthermore, when b is a white noise, the previous estimate is optimal.

$$g * f = FFT^{-1}\left(FFT[g]\overline{FFT[f]}\right) \tag{4}$$

The use of the 'shifting' property enables one to 'move' a signal. For the sake of simplicity, let us consider the shift operator T_d defined for 1D signals $[T_d f](\xi) = f(\xi - d)$, where d is the shift parameter. The FFT of $T_d f$ becomes $FFT[T_d f] = E_d FFT[f]$, where the modulation operator E_d is defined by,

$$[E_d f](\xi) = \exp(-2\pi j \partial \xi) f(\xi). \tag{5}$$

These two results are the basic tools used for image correlation [29].

3.2 CORRELATION ALGORITHM FOR TWO DIMENSIONAL SIGNALS: CORRELI^{2D}

In CORRELI [23] algorithm, two images, referred to as 'reference image' and 'deformed image' as shown in Fig.1(a) and Fig.1(b) respectively are considered for strain computation. A region of interest (ROI) of size $2^p \times 2^p$ pixels centered in the reference image is selected as shown in Fig.2. The ROI is composed of a number of random elementary regions called ZOIs. The ROI of the same size as in the reference image is selected in the deformed image. A first FFT correlation between the two ROIs results into the average displacement U_0, V_0 of the deformed image with respect to the reference image. The maximum of the cross correlation function evaluated for each pixel of the respective ROI is expressed as integer number of pixels representing the shift between the two ROIs. The correlation predicts the maximum number of common pixels between the ROIs. The ROI in the deformed image is now

centered at a point corresponding to the displaced center of the ROI in the reference image by an amount U_0, V_0. In the next step, in order to track the shift for the ZOIs in the reference image, elementary square ZOIs of size $2^s \times 2^s$ pixels where $s < p$ are selected in the reference image as shown in Fig.2. In order to map the whole image, the shift $\delta_x(= \delta_y)$ should be chosen careful such that the shift between two consecutive ZOIs is $1 \le \delta_x \le 2^s$ pixels. These two parameters define the mesh formed by the centers of each ZOI used to analyze the displacement field. Further, the following analysis is performed for each ZOI independently in order to compute the strain for all the ZOIs.

A first FFT correlation of the reference ZOI is carried out with the ROI of the deformed image in order to spot the corresponding ZOI. The correlation results into in plane integral displacement of ΔU, ΔV for the reference ZOI. The displacement correction for the ZOI is completed by displacing the reference ZOI by an additional amount ΔU, ΔV. To limit the errors due to edge effects the considered ZOI is then windowed by a modified Hanning window:

$$\overline{ZOI} = ZOI(H \otimes H) \tag{7}$$

where, $\overline{ZOI}$ denotes the windowed ZOI, $\otimes$ the dyadic product and H the one dimensional modified Hanning window,

$$H(i) = \begin{cases} \dfrac{1}{2}\left[1 - \cos\left(\dfrac{4\pi i}{2^s - 1}\right)\right] & \text{when } 0 \le i \le 2^{s-2} \\ 1 & \text{when } 2^{s-2} \le i \le 3 \times 2^{s-2} \\ \dfrac{1}{2}\left[1 - \cos\left(\dfrac{4\pi i}{2^s - 1}\right)\right] & \text{when } 3 \times 2^{s-2} \le i \le 2^s - 1 \end{cases} \tag{8}$$

The value 2^{s-2} is considered as an optimal value to minimize the error due to edge effects and to have a sufficiently large number of data unaltered by the window [56].

The displacement residues are now less than ½ pixels in each direction. A sub-pixel iterative scheme is used further to pin point the position of ZOI by computing the remaining displacement. A sub-pixel correlation of the displacement δU, δV is determined by evaluating the maximum of a parabolic interpolation of the respective correlation function. The interpolation is performed by considering the maximum pixel and its eight neighboring pixels. By using the 'Shifting-modulation' property of the Fourier Transform one can move the deformed ZOI by an amount - δU, - δV. Since an interpolation was used, one may induce some errors requiring re-iterating by considering the new 'deformed' ZOI until a convergence is reached. The criterion checks the increase in the maximum value of the correlation function with the increase in the number of iterations. Otherwise, the iteration scheme is stopped.

4. RESULTS

The strain on the superficial muscles of the forearm resulting due to calf stretching is evaluated by DIC using cross correlation FFT analysis between the referred and the deformed images. FFT computation between two images, an intermediate step of the algorithm is performed using windows of variable sizes. The simulations are evaluated on an Intel Core 2 Duo 2.20 GHz

machine. The zone of interest from the reference image shown in Fig.1(a) is convoluted with each region of interest in the deformed image as shown in Fig.1(b), in order to locate the shifted position of the reference zone of interest. A high greyscale peak is obtained on convolution of the reference zone of interest with its shifted copy in the deformed image. Once the zone of interest is located in the deformed image the strain can be computed. The strain fields in both the directions are computed with respect to the reference point marked on the leg as shown in Fig.1(a). The reference point refers to the point with respect to which all the strain fields are measured. The results are finally analyzed accordingly.

In order to extract the feature points from the image, dilation in a specified 11×11 square neighborhood is applied for the enlargement or expansion of region of interest as shown in Fig.4(a). In the next step, a threshold of gray scale 50 is applied to extract all the feature points below the respective value. The feature point's colored black can be extracted easily as they have a grayscale of zero and appear as white or binary 1 on inversion while the background turns black as shown in Fig.4(b). The process is explained in detail in the flow chart shown in Fig.5. The feature points are extracted using the Matlab pseudo code shown in Fig.6 (a). Once the feature points have been extracted the strain can be computed by using FFT convolution between the reference and deformed images. The Matlab pseudo code for the FFT cross correlation is shown in Fig.6(b).
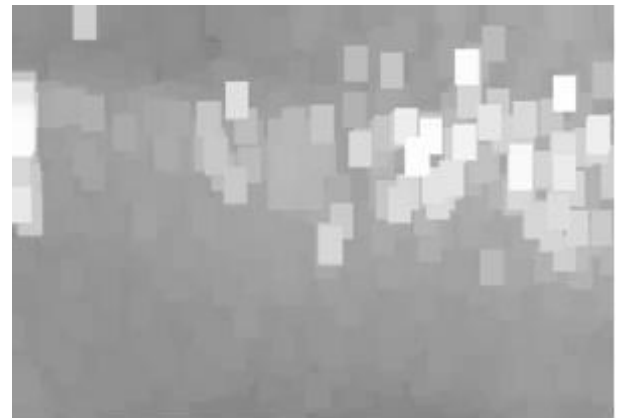
(a)
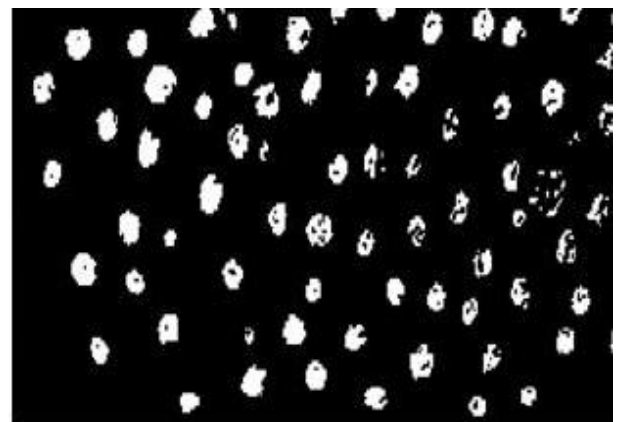
(b)

Fig.4(a). Enlargement of area after square 11×11 Dilation; 4(b) Marker points after thresholding

(c)

Fig.6.(a) Code for extracting the feature points and for computing cross correlation between the two images; (b) Intermediate Cross Convolution FFT Step for DIC algorithm; (c) High greyscale peak observed on convolution between two ZOIs

Flow chart (Fig.5)

Body Part

↓

Zinc coating

↓

Random Speckle Pattern

↓

Images captured by camera

↓

Pre-processing step (Dilation)
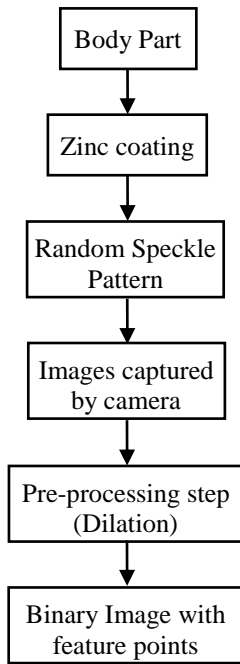
↓

Binary Image with feature points

Fig.5. Flow chart for Feature Extraction

In order to compute the shift between two images, a square ROI of size 512×512 pixels is considered in the reference image, to cover maximum number of pixels. A variable zone of interest is considered by computing the height and width of the patch. A total of 64 ZOI are considered for correlation between both the images. On convolution between the images, a high grayscale is observed when the reference zone of interest in the reference image is convoluted with the same zone of interest in the deformed image as shown in Fig.6(c). The reference ZOI is correlated with every ZOI of the deformed image. A high gray scale value of 247 is observed on correlation of reference ZOI with its shifted copy in the deformed image. The minute displacement of 64 pixels in each direction is evaluated by determining the maximum of a parabolic interpolation of the correlation function after minimizing the errors due to edge effects. The interpolation is performed by considering the maximum pixel and its eight neighbours. Therefore after obtaining a sub-pixel value, the ZOI is shifted using the 'Shifting' property of the Fourier transform. The process is re-iterated in order to avoid the errors due to parabolic interpolation. The pseudo code can be used to calculate the shift between two consecutive images. $D2$ and $D1$ represent the reference and deformed grayscale images respectively, while g^2 is the resulting correlation, between the two images as shown in Fig.6(b).

Pseudo Code

```
I=imread();
I-imresize(I..25);
D=rgb2gray(I);
se1=strel('square'.11);
K=imdilate(D . se1);
P=D(:,:) < 50;
```
(a)

Pseudo Code

```
D1 = Image1;
D2 = Image2;
g2=ifft2((fft2((D1))).*fft2((D2)));
```
(b)
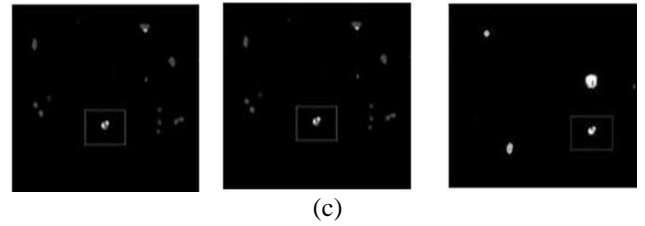
Strain field can be easily computed once the shifted ZOI has been located in the deformed image. The strain is computed using the strategy described in Fig.7. The strain along Y-plane is computed along Y-axis as shown in Fig.1(a). The strain is evaluated along a line *a-b* formulated in a way such that one end of the line is near the reference point while the other is near the ankle as shown in Fig.8(a). The point '*a*' corresponds to the point near to the ankle while point '*b*' is the farther end on the line a-b. When the calf is stretched the gastrocnemius tendon and aponeurosis are stretched. The strain field is observed to be maximum at point '*a*' as the flexor tendons experience the utmost stretch in close proximity to the foot while minimum at the farthest end of the line at point '*b*' as the stretch in the tendons goes on decreasing while moving towards the knee away from the ankle. The statement is supported by the Y- plain strain field plot as shown in Fig.8(a). The highest strain of 0.167 mm is experienced by point '*a*' while the strain is minimum at point '*b*' with a value of 0.128 mm.

The strain field along X-plane is computed along X-axis as shown in Fig.1(a). The strain is evaluated along a line *c-d* formulated in a way such that one end of the line is near the ankle in the area having high strain. The point '*c*' represents the point near to the ankle while the point '*d*' corresponds to the distant end on the line *c-d*. The strain field in the X-plane is extremely small as compared to the strain field experienced by the tendons in the Y- plane. Point '*c*' is relatively near to the ankle as compared to point '*d*' as a result of which the strain is supplementary at point '*c*' as compared to the farthest end point '*d*' along the line *c-d*. The stretch in the tendons goes on decreasing as we move towards the foot in the similar way compared to Y-plane. The above statements are supported by the X-plane strain field plot as shown in Fig.8(b). The highest strain of 0.0018 mm is experienced at point '*c*' while the minimum strain at point '*d*' with a value of 0.002 mm.

5. CONCLUSION

The section presents a brief summary of the generic methodology applied to measure the strain due to calf stretching. The paper presents a generic methodology to compute the strain pattern for calf stretching experiment, a remedy for tarsal tunnel syndrome. It is extremely important as well as essential to understand the contraction and elongation behavior of the superficial flexor tendons as the primary knowledge gained will assists us to generate muscle-tendon units which can resulting into better understanding of the force and energy production. The simulations can be further used to get relevant information

regarding input parameters for simulation models of the human system as well as to examine adaptation phenomena of tendons and aponeuroses to physical activity. This system will help physiotherapists, surgeons and practitioners to educate themselves and refine their work related to TTS.

physiotherapists, surgeons and practitioners to educate themselves and refine their work related to TTS.
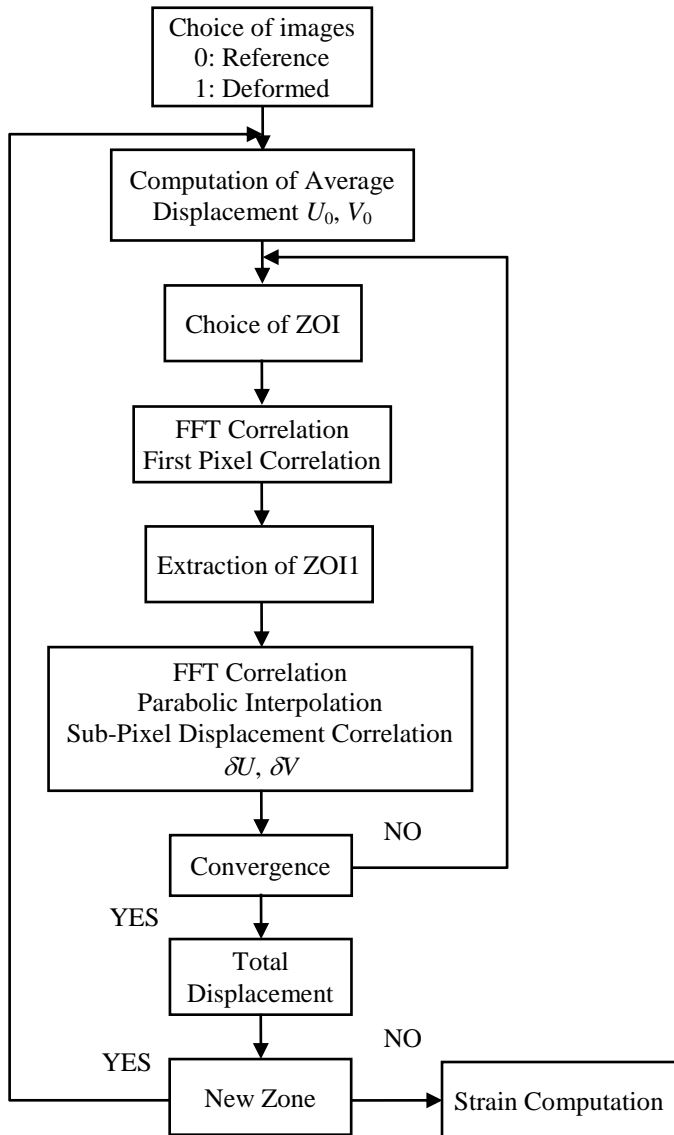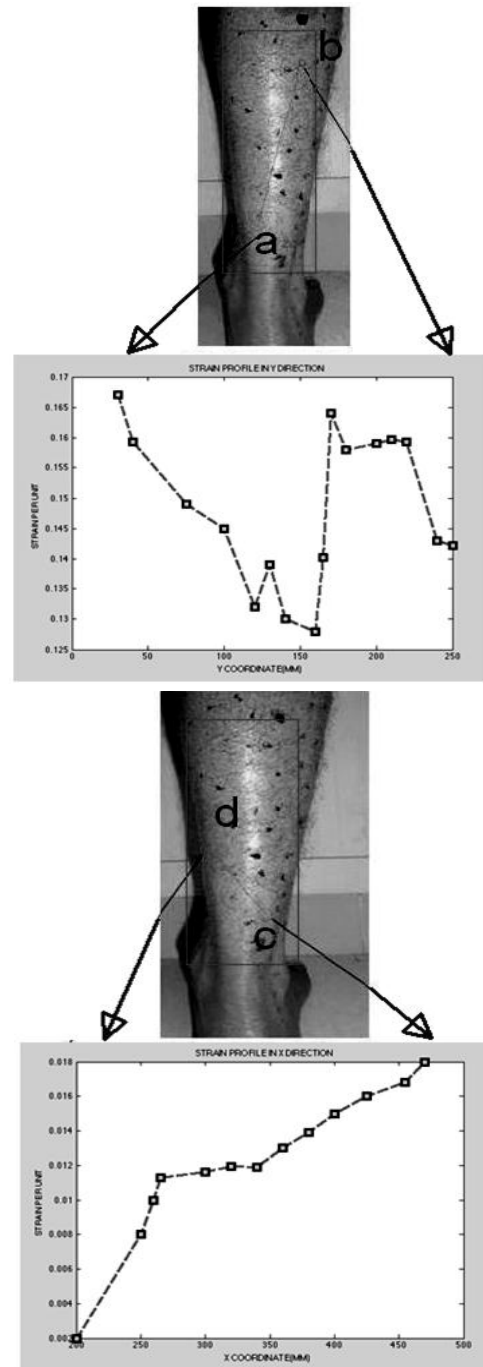
Fig.7. Flow chart for strain computation

6. CONCLUSION

The section presents a brief summary of the generic methodology applied to measure the strain due to calf stretching. The paper presents a generic methodology to compute the strain pattern for calf stretching experiment, a remedy for tarsal tunnel syndrome. It is extremely important as well as essential to understand the contraction and elongation behavior of the superficial flexor tendons as the primary knowledge gained will assists us to generate muscle-tendon units which can resulting into better understanding of the force and energy production. The simulations can be further used to get relevant information regarding input parameters for simulation models of the human system as well as to examine adaptation phenomena of tendons and aponeuroses to physical activity. This system will help

Fig.8(a) Strain Field in the Y plane; (b) Strain Field in the X plane

REFERENCES

[1] Charles Keck, "The Tarsal-Tunnel Syndrome", *The Journal of Bone & Joint Surgery*, Vol. 44, No. 1, pp. 180-182, 1962.

[2] Stephan Maibaum, Markus Braun, Bernd Jagomast and Karel Kučera, "Tarsal –Tunnel-Syndrome", 10.1007/3-540-33523-4_21.

[3] Joe Godges, Robert Klingman, Loma Linda and KPSoCal, "Ankle Nerve Disorder"

http://xnet.kp.org/socal_rehabspecialists/ptr_library/09Foot Region/07Ankle&Foot-RadiatingPain.pdf.

[4] Catherine E. Patla and Haxby Abbott, "Tibialis Posterior Myofascial Tightness as a Source of Heel Pain: Diagnosis and Treatment", *Journal of Orthopaedic & Sports Physical Therapy*, Vol. 30, No. 10, pp. 624-632, 2000.

[5] Bailie D. S and Kelikian A. S, "Tarsal tunnel syndrome: diagnosis, surgical technique, and functional outcome", *Foot & Ankle International*, Vol. 19, No. 2, pp. 65-72, 1998.

[6] M. O'donnell, Skovoroda A. R, Shapo B. M, and Emelianov S. Y, "Internal displacement and strain imaging using ultrasonic speckle tracking," *IEEE Transactions on Ultrasonics, Ferroelectrics and Frequency Control*, Vol. 41, No. 3, pp. 314–325, 1994.

[7] P. Chaturvedi, M. F. Insana and T. J. Hall, "2-D companding for noise reduction in strain imaging", *IEEE Transactions on Ultrasonics, Ferroelectrics and Frequency Control*, Vol. 45, No. 1, pp. 179–191, 1998.

[8] X. C. Chen, M. J. Zohdy, S. Y. Emelianov and M. O'donnell, "Lateral speckle tracking using synthetic lateral phase", IEEE Transactions on Ultrasonics Ferroelectrics and Frequency Control, Vol. 51, No. 5, pp. 540–550, 2004.

[9] J. D'hooge, A. Heimdal, F. Jamal, T. Kukulski, B. Bijnens, F. Rademakers, L. Hatle, P. Suetens, and G. R. Sutherland, "Regional strain and strain rate measurements by cardiac ultrasound: principles, implementation and limitations", *European Journal of Echocardiography*, Vol. 1, No. 3, pp. 154–170, 2000.

[10] B. S Garra, E. I. Cespedes, J. Ophir, S. R. Spratt, R. A. Zuurbier, C. M. Magnant, and M. F. Pennanen, "Elastography of breast lesions: Initial clinical results," *Radiology*, Vol. 202, No. 1, pp. 79–86, 1997.

[11] E. E. Konofagou, T. Varghese and J. Ophir, "Theoretical bounds on the estimation of transverse displacement, transverse strain and poisson's ratio in elastography", *Ultrasonic Imaging*, Vol. 22, No. 3, pp. 153–177, 2000.

[12] A. Thitaikumar, T. A. Krouskop, B. S. Garra and J. Ophir, "Visualization of bonding at an inclusion boundary using axial-shear strain elastography: a feasibility study", *Physics in Medicine and Biology*, Vol. 52, No. 9, pp. 2615–2633, 2007.

[13] R. Ahlgren, M. Cinthio, S. Steen, H. W. Persson, T. Sjoberg, and K. Lindstrom, "Effects of adrenaline on longitudinal arterial lopata et al.: estimation of strain in shearing and rotating structures 863wall movements and resulting intramural shear strain: a first report," *Clinical Physiology and Functional Imaging*, Vol. 29, No. 5, pp. 353–359, 2009.

[14] W. Han, M. X. Xie, X. F. Wang, Q. Lu, J. Wang, L. Zhang and J. Zhang, "Assessment of left ventricular torsion in patients with anterior wall myocardial infarction before and after revascularization using speckle tracking imaging", *Chinese Medical Journal (English)*, Vol. 121, No. 16, pp. 1543–1548, 2008.

[15] Kirkpatrick S, Schroeder M and Simons, J, "Evaluation of Passenger Rail Vehicle Crashworthiness", *International Journal of Crashworthiness*, Vol. 6, No. 1, pp. 95-106, 2001.

[16] Marzougui D, Eskandarian A and Mechzkowski L, "Analysis and Evaluation of a Redesigned 3" x 3" Slipbase Sign Support System Using Finite Element Simulations", *International Journal of Crashworthiness*, Vol. 4, No. 1, 1999.

[17] Watanabe K, Koseki J and Tateyama M, "Application of High-Speed Digital CCD Cameras to Observe Static and Dynamic Deformation Characteristics of Sand", *Geotechnical Testing Journal*, Vol. 28, No. 5, pp. 423-435, 2005.

[18] Thurner P J, Erickson B, Jungmann R, Schriiock Z, Weaver J. C, Fantner G. E, Schitter G, Morse D. E and Hansma P. K, "High-Speed Photography of Human Trabecular Bone during Compression", *Materials Research Society Symposium Proceedings*, Vol. 874, pp. 97-102, 2005

[19] A. Walker, "Moiré interferometry for strain analysis", *Optics and Lasers in Engineering*, Vol. 8, No. 3-4, pp. 213-262, 1988.

[20] T. Puškar, D. Jevremović, L. Blažić, D. Vasiljević, D. Pantelić, B. Murić and B. Trifković, " Holographic interferometry as a method for measuring strain caused by polymerization shrinkage of dental composite", *Contemporary Materials*, I–1, pp. 105-111, 2010.

[21] A. R. Luxmoore, F. A. A. Amin and W. T. Evans, "In-plane strain measurement by speckle photography: A practical assessment of the use of Young's fringes", *The Journal of Strain Analysis for Engineering Design*, Vol. 9, No. 1, pp. 26-35, 1974.

[22] Ziegahn K, Lichtenberger R and Schreier H, "Contactless and full-field 3D-deformation measurement for impact and crash tests", *Proceedings of 7th International Symposium and Exhibition on Sophisticated Car occupant Safety Systems*, 2004.

[23] Peters W. H and Ransom W. F, "Digital Imaging techniques in experimental analysis", *Optical Engineering*, Vol. 21, No. 3, pp 427 – 431, 1982.

[24] Herd F. Perie J. N and Coret M, "Mesure de champs de de-placements 2D par Interpolation D'images: CORRELI", internal repot (LMT-cachan), Vol. 230, 1999.

[25] Sutton M. A, Cheng M, Peters W. H, Chao Y. J and McNeill S. R, "Application of an optimized digital correlation method to planar deformation analysis", *Image and Vision Computing*, Vol. 4, No. 3, pp. 143-151, 1986.

[26] Kevin M. Moerman, Cathy A. Holt, Sam L. Evans and Ciaran K. Simms, "Digital image correlation and finite element modelling as a method to determine mechanical properties of human soft tissue in vivo", *Journal of Biomechanics*, Vol. 42, No. 8, pp. 1150-1153, 2009.

[27] Wang C. C. B, Deng J. M, Ateshian G. A and Hung C. T, "An automated approach for direct measurement of two-dimensional strain distributions within articular cartilage

under unconfined compression", *Journal of Biomechanical Engineering*, Vol. 124, No. 5, pp. 557–567, 2002.

[28] Nicolella D. P, Moravits D. E, Gale A. M, Bonewald L. F and Lankford J, "Osteocyte lacunae tissue strain in cortical bone", *Journal of Biomechanics*, Vol. 39, No. 9, pp. 1735–1743, 2006.

[29] Thompson M S, Schell H, Lienau J and Duda G N, "Digital image correlation: A technique for determining local mechanical conditions within early bone callus", *Medical Engineering & Physics*, Vol. 29, No. 7, pp. 820–823, 2007.

[30] Zhou P and Goodson K. E, "Sub-pixel Displacement and Deformation Gradient Measurement Using Digital Image-Speckle Correlation (DISC)", *Optical Engineering*, Vol. 40, No. 8, pp 1613-1620, 2001.

[31] Vogel D, Grosser V, Schubert A and Michel B, "MicroDAC Strain Measurement for Electronics Packaging Structures", *Optics and Lasers in Engineering*, Vol. 36, No. 2, pp. 195-211, 2001.

[32] Srinivasan V, Radhakrishnan S, Zhang X, Subbarayan G, Baughn T and Nguyen L, "High Resolution Characterization of Materials Used In Packages Through Digital Image Correlation", *Proceedings of ASME/Pacific Rim Technical Conference and Exhibition on Integration and Packaging of MEMS, NEMS and Electronic Systems*, pp. 17-22, 2005.

[33] Sutton M. A, Cheng M, Peters W. H, Chao Y. J and McNeill S. R, "Application of an optimized digital correlation method to planar deformation analysis", *Image and Vision Computing*, Vol. 4, No. 3, pp. 143-151, 1986.

[34] Reu P and Miller T, "High-speed Multi-camera DIC for Finite Element Model Validation", *Proceedings of the SEM Annual Conference and Exposition on Experimental and Applied Mechanics*, 2006.

[35] Tiwari V, Williams S, Sutton M and McNeill S, "Application of Digital Image Correlation in Impact Testing", *Proceedings of the SEM Annual Conference and Exposition on Experimental and Applied Mechanics*, 2005.

[36] Kehoe L, Lynch P and Guénebaut V, "Measurement of Deformation and Strain in First Level C4 Interconnect and Stacked Die using Optical Digital Image Correlation", *Proceedings of Electronic Components and Technology Conference*, pp. 1874-1881, 2006.

[37] Cheng T, Dai C and Gan R, "Viscoelastic Properties of Human Tympanic Membrane", *Annals of Biomedical Engineering*, Vol. 35, No. 2, pp. 305-314, 2007.

[38] Myers K. M, Paskaleva A. P, House M and Socrate S, "Mechanical and biochemical properties of human cervical tissue", *Acta Biomaterialia*, Vol. 4, No. 1, pp. 104-116, 2008.

[39] Boyce B. L, Grazier J. M, Jones R. E and Nguyen T. D, "Full-field deformation of bovine cornea under constrained inflation conditions", *Biomaterials*, Vol. 29, No. 28, pp. 3896-3904, 2008.

[40] Sutton M. A, Ke X, Lessner S. M, Goldbach M, Yost M, Zhao F and Schreier H. W, "Strain field measurements on mouse carotid arteries using microscopic three-dimensional digital image correlation", *Journal of Biomedical Materials Research Part A*, Vol. 84, No. 1, pp. 178-190, 2008.

[41] Bonetto P, Comis G, Formiconi A R and Guarracino M. A, "A new approach to brain imaging, based on an open and distributed environment", *Proceedings of First International IEEE EMBS Conference on Neural Engineering*, pp. 521-524, 2003.

[42] Chu T. C, Ranson W. F, Sutton M. A and Petters W. H, "Applications of Digital-Image-Correlation Techniques to Experimental Mechanics", *Experimental Mechanics*, Vol. 25, No. 3, pp. 232-244, 1985.

[43] Chiang F.P, Wang Q and Lehman F, "New developments in full-field strain measurements using speckles", *In Non-traditional Methods of Sensing Stress, Strain and Damage in Materials and Structures*, pp 156–169, 1997.

[44] Chen J, Xia G, Zhou K, Xia G and Qin Y, "Two-step digital image correlation for micro-region measurement, Optics and Lasers in Engineering, Vol. 43, No. 8, pp. 836–846, 2005.

[45] Zhang Z F, Kang Y L, Wang H W, Qin Q H, Qiu Y and Li X Q, "A novel coarse–fine search scheme for digital image correlation method", *Measurement*, Vol. 39, No. 8, pp. 710–718, 2006.

[46] Wang M, Wang H and Cen Y, "High-speed digital-image correlation method", *Optics Letters*, Vol. 34, No. 13, pp 1955–1957, 2009.

[47] Amarjot Singh and S. N. Omkar, "Digital Image Correlation using GPU Computing", *International Journal of Biomedical Science and Engineering,* Vol. 1, No. 1, pp. 1-10, 2013.

[48] S. N. Omkar, G. B. Praveen and Amarjot Singh, "An Analysis of Wrist Extension using 3D Digital Image Correlation", *International Journal of Biomedicine and Biotechnology*, Vol. 1, No. 1, pp. 1-7, 2013.

[49] Amarjot Singh and S. N. Omkar, "Analysis of Wrist Extension using Digital Image Correlation", ICTACT Journal on Image and Video Processing, Vol. 2, No. 3, pp. 343-351, 2012.